Title

Nogo receptor blockade overcomes remyelination failure after white matter stroke and stimulates functional recovery in aged mice

Journal

Proceedings of the National Academy of Sciences of the United States of America, 113(52)

ISSN

0027-8424

Authors

Sozmen, Elif G
Rosenzweig, Shira
Llorente, Irene L
et al.

Publication Date

2016-12-27

DOI

10.1073/pnas.1615322113

Peer reviewed

Nogo receptor blockade overcomes remyelination failure after white matter stroke and stimulates functional recovery in aged mice

Elif G. Sozmen[a,1], Shira Rosenzweig[a,1], Irene L. Llorente[a], David J. DiTullio[a], Michal Machnicki[a], Harry V. Vinters[b], Lief A. Havton[a], Roman J. Giger[c], Jason D. Hinman[a], and S. Thomas Carmichael[a,2]

[a]Department of Neurology, David Geffen School of Medicine at UCLA, Los Angeles, CA 90095; [b]Department of Neuropathology, David Geffen School of Medicine at UCLA, Los Angeles, CA 90095; and [c]Department of Cell and Developmental Biology, University of Michigan School of Medicine, Ann Arbor, MI 48109

Edited by Fred H. Gage, The Salk Institute for Biological Studies, San Diego, CA, and approved November 8, 2016 (received for review September 19, 2016)

White matter stroke is a distinct stroke subtype, accounting for up to 25% of stroke and constituting the second leading cause of dementia. The biology of possible tissue repair after white matter stroke has not been determined. In a mouse stroke model, white matter ischemia causes focal damage and adjacent areas of axonal myelin disruption and gliosis. In these areas of only partial damage, local white matter progenitors respond to injury, as oligodendrocyte progenitors (OPCs) proliferate. However, OPCs fail to mature into oligodendrocytes (OLs) even in regions of demyelination with intact axons and instead divert into an astrocytic fate. Local axonal sprouting occurs, producing an increase in unmyelinated fibers in the corpus callosum. The OPC maturation block after white matter stroke is in part mediated via Nogo receptor 1 (NgR1) signaling. In both aged and young adult mice, stroke induces NgR1 ligands and down-regulates NgR1 inhibitors during the peak OPC maturation block. Nogo ligands are also induced adjacent to human white matter stroke in humans. A Nogo signaling blockade with an NgR1 antagonist administered after stroke reduces the OPC astrocytic transformation and improves poststroke oligodendrogenesis in mice. Notably, increased white matter repair in aged mice is translated into significant poststroke motor recovery, even when NgR1 blockade is provided during the chronic time points of injury. These data provide a perspective on the role of NgR1 ligand function in OPC fate in the context of a specific and common type of stroke and show that it is amenable to systemic intervention to promote recovery.

repair | oligodendrocyte progenitor cell | oligodendrocyte | subventricular zone | astrocyte

Ischemic stroke in the adult brain occurs in two basic forms. Occlusion of large brain arteries produces stroke that spans brain areas, including gray matter (cortex, striatum) and white matter regions. Stroke in small brain vessels often occurs only in subcortical white matter regions, and these infarcts account for up to 25% of all stroke. The incidence of white matter stroke is age-associated and is the second leading cause of dementia (1–3). The resulting infarcts are distinct from large artery stroke, not only in cause and location but also in progressive accumulation over time (1, 3, 4). Ischemic regions after white matter stroke grow, with progression of the damage even in the controlled conditions of a clinical trial (5). Importantly, the presence of white matter ischemic lesions closely correlates with abnormalities in cognition, balance, and gait and carries an increased risk of death (6, 7).

Despite such clinical importance, white matter repair after white matter stroke is still relatively unknown, which is in part because most basic science studies of stroke focus on large artery infarcts, such as middle cerebral artery occlusions. Most of what is known about white matter repair is derived from studies in inflammatory or toxic injuries of white matter, such as multiple sclerosis (MS). In these nonstroke demyelinating lesions, a repair process is characterized by an initial regenerative response that remyelinates surviving axons. In MS models of disease, oligodendrocyte progenitors (OPCs) respond to the injury, proliferate, and mature into myelinating oligodendrocytes (OLs), which restore some amount of lost function (8, 9). In MS models, OPCs are recruited from the subventricular zone (SVZ) to areas of white matter damage (10, 11). Later, failure of this OPC regenerative response may lead to the accumulating effect of MS (8, 9). Unlike MS, stroke kills all cell types within the white matter and creates a microenvironment that is different from the immune-mediated pathology. Initial studies in this field indicate that OLs undergo a profound morphological change after large artery stroke (12). However, whether OPCs can migrate to areas of injury, differentiate into OLs, and partially repair the ischemic lesion remain to be described. Such fundamental questions regarding repair in white matter stroke hold the potential for new stroke-specific therapies that can reduce the burden of this disease.

We investigated the mechanisms of ischemic white matter repair by using transgenic mice, cellular fate mapping, viral vector-based cell tracking, and structural and behavioral measures of white matter repair in aged animals. Our data indicate that, unlike the inflammatory lesions of MS, there is no initial remyelination response in white matter stroke, even in the candidate repair zone where axons are intact. We find that local OPCs proliferate and that a portion differentiate into astrocytes, with the remaining cells blocked in a progenitor phenotype. White matter stroke alters the expression profile of molecules that signal within the NgR1 system in both mouse and human white matter stroke, with a special

Significance

White matter stroke is a common clinical problem that leads to widespread cognitive and sensorimotor deficits. The incidence of white matter stroke is sharply age-associated; imaging studies indicate that, over age 80, virtually all of us will have white matter strokes. Little is known of the repair processes after white matter stroke. Here, we report the tissue repair processes after white matter stroke and identify Nogo receptor 1 (NgR1) ligands as inhibitors. We show that white matter repair and functional recovery are indeed possible in aged brains when an engineered NgR1 decoy receptor is systemically administered after white matter stroke, even at chronic periods in this disease.

Author contributions: E.G.S., S.R., I.L.L., D.J.D., R.J.G., J.D.H., and S.T.C. designed research; E.G.S., S.R., I.L.L., D.J.D., M.M., L.A.H., and J.D.H. performed research; E.G.S., S.R., I.L.L., D.J.D., H.V.V., J.D.H., and S.T.C. analyzed data; and E.G.S., S.R., I.L.L., and S.T.C. wrote the paper.

The authors declare no conflict of interest.

This article is a PNAS Direct Submission.

Freely available online through the PNAS open access option.

[1]E.G.S. and S.R. contributed equally to this work.

[2]To whom correspondence should be addressed. Email: scarmichael@mednet.ucla.edu.

This article contains supporting information online at www.pnas.org/lookup/suppl/doi:10.1073/pnas.1615322113/-/DCSupplemental.

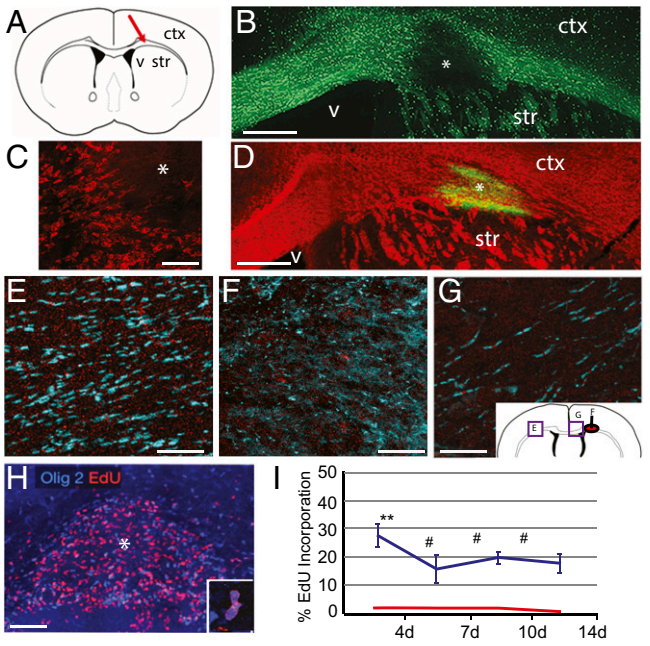

Fig. 1. White matter stroke model and progenitor response. (*A*) Location for L-NIO injection into subcortical white matter is indicated by arrow. (*B*) Loss of GFP expressing oligodendrocytes in the PLP-GFP transgenic line 7 d after stroke. The green fluorescence is within PLP-expressing OLs or late-stage OL-lineage cells. Asterisk denotes center of stroke. (*C*) Loss of CC1$^+$ cells. Asterisk denotes stroke site. (*D*) Serum-derived IgG (green) and axonal neurofilaments (NF200, red) indicate the region of BBB breakdown and IgG diffusion into brain. The NF200 stain indicates the surround to the stroke, showing that the BBB is opened at the stroke site and adjacent white matter. (*E* and *G*) Paranodes and nodes of Ranvier are visualized by Caspr (blue) and βIV-spectrin (red). Healthy white matter (*E*) shows the normal tripartite architecture of paranode–node–paranode in closely packed axons. The stroke core (*F*) lacks both markers, consistent with axonal loss. The peri-infarct white matter (*G*) exhibits relatively preserved nodal architecture. (*G*, *Inset*) The location of images for *E*–*G*. (*H*) Olig2 immunoreactive cells (blue) in section stained for EdU (red) that includes the stroke core and adjacent white matter. (*Inset*) Higher-magnification of colocalization of Olig2/EdU in this pulse-labeling protocol. (*I*) Percentage of Olig2$^+$ cells that incorporated EdU over the total number of Olig2$^+$ cells. $^{\#}P < 0.0001$ in all time points. The *y* axis is days after stroke. **4 d vs. 7 d, $P < 0.001$; 4 d vs. 14 d, $P < 0.001$. $n = 5$. ctx, cortex; str, striatum; v, ventricle. (Scale bars: *B* and *D*, 100 μm; *C*, 25 μm; *E*–*G*, 20 μm; *H*, 30 μm.)

effect of age. Antagonism of NgR ligands by systemic delivery of a soluble receptor body, NgR(OMNI)-Fc, alleviates the OPC differentiation block, reduces the number of OPCs that shunt into astrocytes, and produces behavioral recovery after stroke in aged mice. Importantly, the beneficial effects of NgR(OMNI)-Fc can be produced at chronic time points after white matter stroke.

Results

OPCs Show Limited Differentiation After White Matter Stroke. Induction of subcortical white matter stroke in the mouse (Fig. 1*A*) leads to loss of oligodendrocytes (Figs. 1 *B* and *D*), disruption of nodes of Ranvier of myelinated axons (Fig. 1 *E*–*G*), and blood–brain barrier (BBB) breakdown (Fig. 1*B*) in processes that are shared between the mouse and the human condition (13–16). Because white matter ischemic lesions progress in humans (17), we assessed progenitor responses after white matter stroke in a stepwise approach. In these studies, we specifically assessed OPC responses in the white matter tissue adjacent to the infarct, in which axons are preserved, termed as "peri-infarct" white matter (Fig. 1*G* and Fig. S1) (13, 15, 16).

The OPC proliferation rate in this stroke model was measured by brief pulses of the S phase marker 5-ethynyl-2′-deoxyuridine (EdU) given shortly after stroke, before euthanasia time points. Cells were costained for oligodendrocyte lineage transcription factor 2 (Olig2), a bHLH transcription factor broadly expressed in OPCs and OLs (18). Newly born, Olig2$^+$ cells filled the infarct and adjacent tissue (Fig. 1*H*). At all poststroke intervals, a significant induction of proliferation in Olig2$^+$ cells was observed (Fig. 1*I*). OPC proliferation was highest at the earliest time point, 4 d after stroke (Fig. 1*I*). Pulse-delivered EdU incorporation in nonstroked adult white matter OPCs was negligible, as anticipated (Fig. 1*I*).

To fully determine the fate of newly proliferated OPCs after white matter stroke, we used a narrow window of EdU administration and an NG2::CreERT2/Rosa-yellow fluorescent protein (YFP) OPC reporter mouse (termed "OPC reporter") (Fig. 2*A*). Tamoxifen-induced Cre led to YFP expression selectively in NG2 cells in white matter, labeling 60% of NG2 and/or PDGFRα immunoreactive OPCs (Fig. 2*B*). No reporter activity was detected in astrocytes, microglia/macrophages, or neurons after Cre activation. NG2 (neural/glial antigen 2) promoter-driven YFP expression can be present in pericytes; however, they are morphologically distinct from OPCs and do not differentiate into glia after CNS injury (19), and YFP$^+$ pericytes did not respond to stroke (Fig. S2).

White matter stroke produced lesions densely populated by YFP$^+$ reporter cells (Fig. 2*C*), which are in the OPC lineage (Olig2$^+$) (Fig. S2*A*). The fate of OPCs after white matter stroke

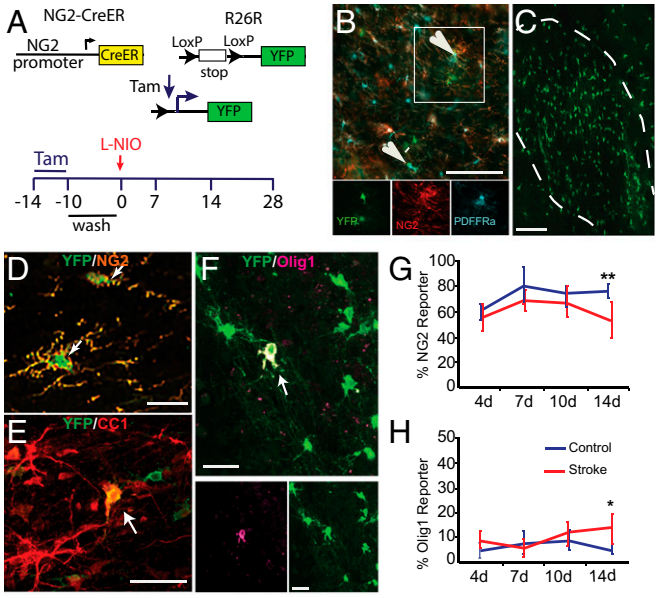

Fig. 2. Genetic fate mapping of OPCs after white matter stroke. (*A*) Tamoxifen-inducible NG2::CreERT2 line is crossed with Rosa-YFP mice to generate the OPC reporter mouse line. Bidaily injections of tamoxifen were given for 5 d to induce recombination. Infarcts were created after a 10-d washout period to reduce the protective effect of tamoxifen against ischemic injury. (*B*) In the absence of injury in the OPC reporter mouse, YFP is detected in cells expressing OPC markers: NG2 and PDGFRα. Arrowheads indicate triple labeled OPCs. (*C*) OPC reporter activity 7 d after stroke seen as YFP$^+$ cells. OPCs fill the stroke core and peri-infarct white matter, which is shown schematically by dashed lines. The stroke core is demarcated as the region of loss of oligodendrocytes (CC1 stain) in adjacent sections. (*D*) Undifferentiated reporter cells, NG2$^+$/YFP$^+$, at 7 d after stroke (arrows). (*E*) NG2 reporter positive cell stained for a maker of a more mature oligodendrocyte, CC1 (arrow). (*F*) YFP$^+$ OPC reporter cell labeled with cytoplasmic Olig1 (arrow). *Bottom* panels show individual fluorescent channels. (*G*) Undifferentiated OPC reporter cells as the percentage of NG2$^+$/YFP$^+$ reporters over the total number YFP$^+$ cells. **14 d stroke vs. 14 d control, $P < 0.001$, $n = 5$–6. (*H*) Reporter cell differentiation as the percentage of Olig1$^+$ YFP$^+$ reporters over the total number of YFP$^+$ cells. *14 d stroke vs. 14 d control, $P < 0.001$, $n = 5$–6. PDGFRα, platelet-derived growth factor receptor alpha; YFP, yellow fluorescent protein. (Scale bars: *B* and *C*, 100 μm; *D*–*E*, 50 μm; *F*, 30 μm.)

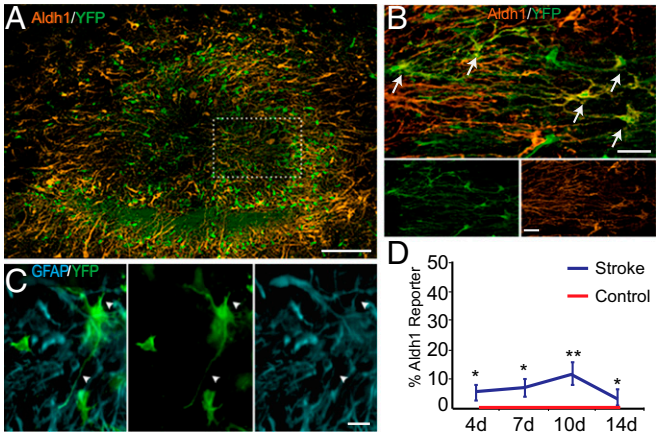

Fig. 3. Astrocytic fate of OPCs after white matter stroke. (*A*) YFP$^+$ OPC reporter cells colabel with the astrocyte marker Aldh1L1 in this low-magnification (100×) view of the infarct. (*B*) Higher magnification (1,000×) of *A* with Aldh1L1$^+$ cells (orange) that are reporter positive (green) appearing as yellow, with characteristic astrocyte morphology (arrows). *Bottom* panels show the individual fluorescent channel. (*C*) GFAP labeling of reporter cells in stroke at day 14. Arrowheads indicate a reporter cell with processes positive for GFAP. (*D*) The percentage of Aldh1L1$^+$ cells that are YFP$^+$ over the total number of YFP$^+$ across the poststroke time points. *P < 0.01, **P < 0.001 stroke vs. control comparison, n = 5–6. (Scale bars: 20 μm.)

was measured in the region of clinical interest, the peri-infarct white matter (Fig. 1*G*), rather than the infarct core in which axons are lost (Fig. 1*F*). Stroked and control OPC reporter brains were stained for NG2 to identify undifferentiated OPCs (Fig. 2*D*); differentiated reporter cells were detected by cytoplasmic translocation of the transcription factor Olig1 (Fig. 2*F*) (18). The majority of the YFP$^+$ cells consisted of uncommitted NG2$^+$ OPCs in both control and stroked white matter at 4–14 d after stroke (Fig. 2*G*). At 14 d after stroke, a significant decrease was observed in the percentage of NG2$^+$ reporter cells relative to nonstroke brains whereas a limited differentiation of OPCs into OLs was noted (Fig. 2 *E* and *F*). We confirmed this substantially limited differentiation of OPCs into OLs during the fate mapping of OPC reporter cells with various OL markers, such as CC1 (Fig. 2*E*) and GST-pi (Fig. S2*B*). There was no change in the overall number of oligodendrocytes over time after stroke in this peri-infarct region (e.g., 7 d control, 6,625 ± 554, stroke 1,347 ± 264; 14 d control, 6,790 ± 400, stroke 1,665 ± 265), indicating that the slight but significant increase in OPCs that mature to oligodendrocytes at 14 d after stroke does not account for a substantial increase in oligodendrocytes in the damaged area.

Previous studies have shown that OPCs can differentiate into neurons and astrocytes in addition to OLs, particularly within cell culture (20). We investigated alternate OPC cell fates after stroke and observed astrocyte fate divergence of OPCs in the peri-infarct white matter as indicated by Aldh1L1-colabeled YFP$^+$ reporter cells (Fig. 3*A* and *B*), constituting 4% to 13% of the total reporter pool across all time points (Fig. 3*D*). This finding was confirmed by glial fibrillary acidic protein (GFAP) labeling of stroke samples (Fig. 3*C*). There was no evidence of astrocytic fate divergence among OPC lineage cells in the absence of stroke (Fig. 3*D*). Importantly, this lack of OPC maturation into OLs and differentiation of OPCs into astrocytes occurred in areas where repair is expected to occur at sites of intact axons adjacent to the infarct. Schwann cell remyelination has been seen in the CNS especially in situations where there is astrocyte loss but preservation of demyelinated axons (21, 22). We stained for a marker of Schwann cell peripheral myelination, periaxin (23), in control and poststroke brains. There was no induction of this peripheral myelin marker in the region of OPC-derived astrocytes (Fig. S3).

SVZ Does Not Contribute to Generation of New OPCs After White Matter Stroke. Responsive OPCs after CNS injury may arise from local white matter progenitors (24), or through migration of progenitors from the subventricular zone (SVZ) (10, 11). The source of OPCs in white matter stroke will have clinical relevance because many of these infarcts lie quite distant from the SVZ in humans (4). To determine whether SVZ contributes to the regenerating OPC pool after stroke, the ipsilateral SVZ was targeted with CMV-GFP lentivirus injection (Fig. 4*A*), which transfects all cell types in the SVZ and allows tracking of the migration and destination of the cells over time (25). In the absence of stroke, SVZ-derived cells formed a collection that is part of the rostral migratory stream, which are negative for the OPC marker NG2 (Fig. 4*B*). GFP labeled cells spanned 600 to 650 μm away from the SVZ in control conditions (Fig. 4*B*). At 7 and 14 d after stroke, no GFP-labeled SVZ cells were found in the proximity of the stroke (Fig. 4*C*), even when the infarct was in close proximity to the virally labeled SVZ (Fig. 4*D*). To confirm the lack of SVZ contribution to OPC regeneration after white matter stroke, the proliferating SVZ pool was labeled before stroke and then dividing cells were tracked. This strategy is different from what was used in poststroke OPC proliferation experiments mentioned above. Systemic administration of EdU using a 5-d pulse before stroke induction labels the shorter cycling time of the transit-amplifying cells in the SVZ that

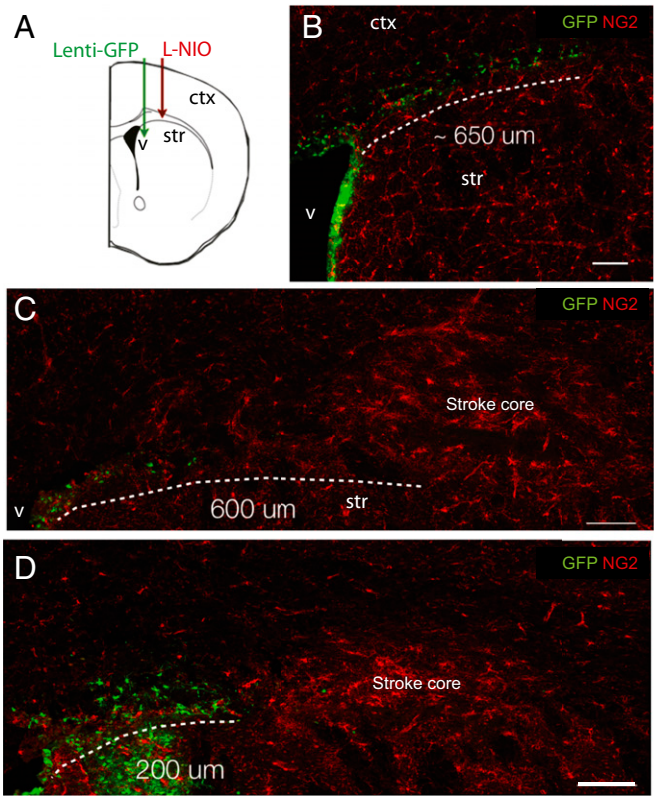

Fig. 4. SVZ does not significantly contribute to OPC regeneration response in white matter stroke. (*A*) Schematic representation of SVZ labeling paradigm. SVZ was targeted by CMV-GFP lentivirus injection 4 d before stroke induction. GFP$^+$ cells were phenotyped at days 7 and 14 after stroke or saline control. ctx, cortex; str, striatum; v, ventricle. (*B*) In the absence of injury, GFP$^+$ cells stream at the border of white matter and dorsal striatum ranging 600–650 μm from SVZ. Cells of SVZ origin were not positive for the OPC marker NG2. (*C* and *D*) GFP$^+$ cells migrating from ipsilateral SVZ do not infiltrate into the lesion or peri-infarct white matter regardless of the proximity of white matter stroke to the SVZ at 7 d (*C*) or 14 d (*D*) after the infarct. The stroke core is demarcated as the region of loss of oligodendrocytes (CC1 stain) in adjacent sections. Lenti, lentivirus. (Scale bars: *B–D*, 100 μm.)

give rise to SVZ-derived OPCs, but not the longer cycling time of local white matter OPCs (26, 27). As expected, the SVZ contained a high number of cells incorporating EdU with this prestroke 5-d labeling protocol (Fig. 5 *D* and *G*). In contrast, the white matter stroke site contained few EdU$^+$ cells (Fig. 5*A*). The EdU$^+$ cells found in the lesion were mostly positive for Iba-1, a microglia/macrophages marker (Fig. 5 *D*–*F*). Additionally, EdU$^+$ cells were rarely positive for Olig2$^+$ OPC lineage cells in white matter stroke (Fig. 5*B*), constituting less than 2% of the total EdU$^+$ pool within the lesion (Fig. 5*C*). In contrast, doublecortin$^+$ cells, which are immature neurons (25), extended from the SVZ into the margins of the white matter stroke (Fig. 5 *D*, *E*, and *G*), indicating that white matter stroke can signal to the SVZ and induce migration of neuronal precursors, but not cells of the OPC lineage. In summary, white matter stroke in the mouse does not induce recruitment of SVZ-derived cells in the OPC lineage, which leaves the resident OPC pool as the most likely contributor to the observed poststroke OPC response.

NgR1 Interactome in White Matter Stroke. These proliferation and fate-tracking studies show that white matter stroke induces a proliferative response from OPCs in the local white matter and that these OPCs are blocked in their ability to differentiate into mature oligodendrocytes in the candidate repair zone. Many molecular signaling systems are described in nonstroke demyelinating studies that may induce OPC proliferation but in turn block OPC differentiation in white matter stroke. For instance, Notch/delta/jagged signaling, extracellular matrix (ECM)-associated hyaluronan sulfate proteoglycans (HSPGs), chondroitin sulfate proteoglycans (CPSGs), Semaphorin 3A, canonical Wnt, and Nogo/NgR1 signaling are some of the candidate systems that may contribute to such an outcome (28–30). Among these, Nogo/NgR1 signaling plays a central role in the differentiation and integration of OPCs (31). NgR1 was originally described as the Nogo receptor 1 for myelin-associated ligands (Nogo, MAG, and OMgp) in axonal growth inhibition, but recent evidence indicates that NgR1 can bind to many molecules in the ECM, including many of the myelin and ECM molecules that modulate OPC differentiation (32). Many of these molecules are differentially regulated in pathological conditions and in the aged brain (33).

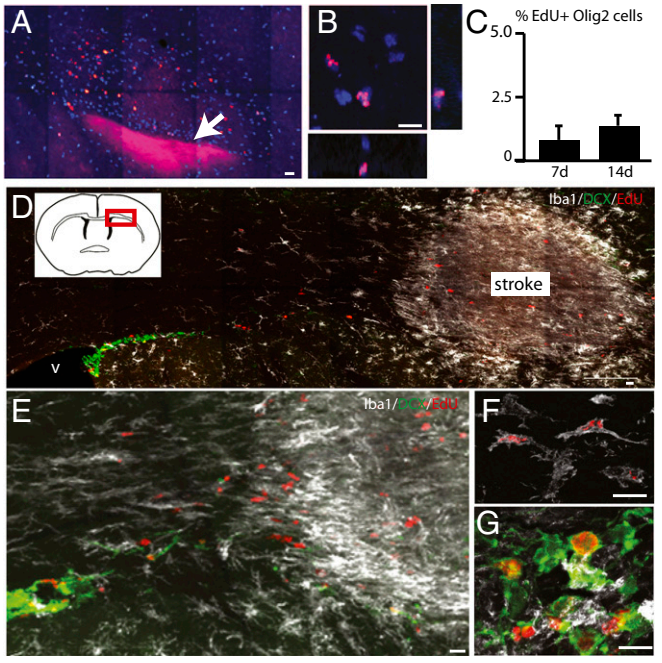

Fig. 5. Cell Proliferation in SVZ in white matter stroke. Bidaily injection of EdU for 5 d before stroke was used to label the progenitor pool in SVZ. (*A*) Few EdU incorporating cells (red) were found in the lesion and were assessed for OPC lineage by anti-Olig2 antibody labeling (blue) at day 7. (*B*) Z plane reconstruction of EdU/Olig2$^+$ cells in a separate section. EdU incorporating Olig2$^+$ cells were rarely observed. (*C*) EdU$^+$ Olig2$^+$ double labeled cells make up less than 2% of total EdU$^+$ cell population in stroke samples. $n = 3$. (*D*) EdU uptake in this paradigm was prominent in ipsilateral SVZ, particularly in DCX$^+$ neuroblasts. IBA-1$^+$ microglia/macrophages surround and fill the stroke site. Schematic shows area of photomicrographs in *D*–*G* in red box. (*E*) Higher-magnification view of stroke margin from a separate tissue section. EdU$^+$ cells cluster near the infarct, largely in the IBA-1$^+$ microglia/macrophages. (*F*) EdU$^+$/IBA-1$^+$ macrophages near infarct border. (*G*) EdU$^+$/DCX$^+$ cells between the infarct border and the SVZ in separate tissue sections. DCX, doublecortin. (Scale bars: *A*, *B*, *D*, and *E*, 10 μm; *F* and *G*, 5 μm.) *A* and *D* are large field of view images assembled from tiled higher-magnification confocal images.

To test whether NgR1 ligands play a role in OPC responses after white matter stroke, we performed quantitative (q)RT-PCR on 28 genes that directly bind to or interact with NgR1 signaling at early (5 d, peak of OPC proliferation) and late (15 d, OPC differentiation block) time points after white matter stroke. We incorporated aged animals in addition to young adults in this study, given that the aging patient population is the most clinically relevant to translational studies of white matter stroke (1, 3). White matter stroke significantly induced CSPG molecules aggrecan, versican, and brevican, and the heparan sulfate proteoglycan core proteins glypican 2 and syndecans 1 and 3 (Fig. 6 and Table S1). There is an age effect observed in that aggrecan, versican, syndecan 1, and glypican 2 are induced to a greater extent in aged stroke. Three negative regulators of NgR1 signaling, leucine-rich glioma inactivated 1 (Lgi1), cartilage acidic protein-1B (LOTUS), and disintegrin and metalloproteinase domain-containing protein 22 (ADAM22) (34, 35), are decreased after white matter stroke, with a greater reduction in aged white matter stroke. Interestingly, white matter stroke reduces levels of NgR1 coreceptor Lingo1 and impressively up-regulates a second myelin protein receptor, paired Ig-like receptor B (PirB) (Fig. 6). Both of these effects are heightened with aged stroke. Expression of NgR1 was measured separately due to low NgR1 RNA levels across experimental groups. NgR1 up-regulation was detected 15 d after white matter stroke, a time point associated with the OPCs differentiation block, but was only significant in young mice, presumably due to overall lower levels of NgR1 in aged mice (Table S2). We selected the three most differentially regulated genes in mouse white matter stroke and determined whether they are present in human white matter stroke samples. PirB, dermatan sulfate epimerase (synthetic enzyme for dermatan sulfate proteoglycan), and versican were induced near the white matter infarcts in human (Fig. S4). Among these, PirB was found to be the most frequently observed within the human peri-infarct white matter, suggestive of a similar inhibitory role in chronic human white matter stroke lesions (Fig. S4).

Antagonism of NgR1 Ligands Promotes Recovery After White Matter Stroke. The gene expression profile in white matter stroke implicates NgR1 signaling in the tissue reorganization after white matter stroke with a particular effect of aging. To study the role of NgR1 ligands in white matter repair, we blocked them in vivo and assessed the effects on OPC differentiation and behavioral recovery. An engineered soluble hybrid of NgR1 and NgR2, NgR(OMNI)-Fc, binds and neutralizes several CNS regeneration inhibitors, including Nogo66, OMgp, and MAG (36). We tested whether neutralizing NgR1 ligands in vivo would overcome the OPC differentiation block in white matter stroke by delivering NgR(OMNI)-Fc into the stroke site of OPC reporter mice. NgR(OMNI)-Fc produced a significant increase in cells with markers of mature OLs compared with the Fc-treated controls (Fig. 7*A*). Also, the number of astrocytes derived from the OPC reporters was markedly reduced in NgR(OMNI)-Fc–injected brains (Fig. 7*B*). The percentage of OPC reporter cells that remained as immature NG2$^+$ pool was not altered in either group (Fig. 7*C*). These data indicate that in vivo blockade of NgR ligands

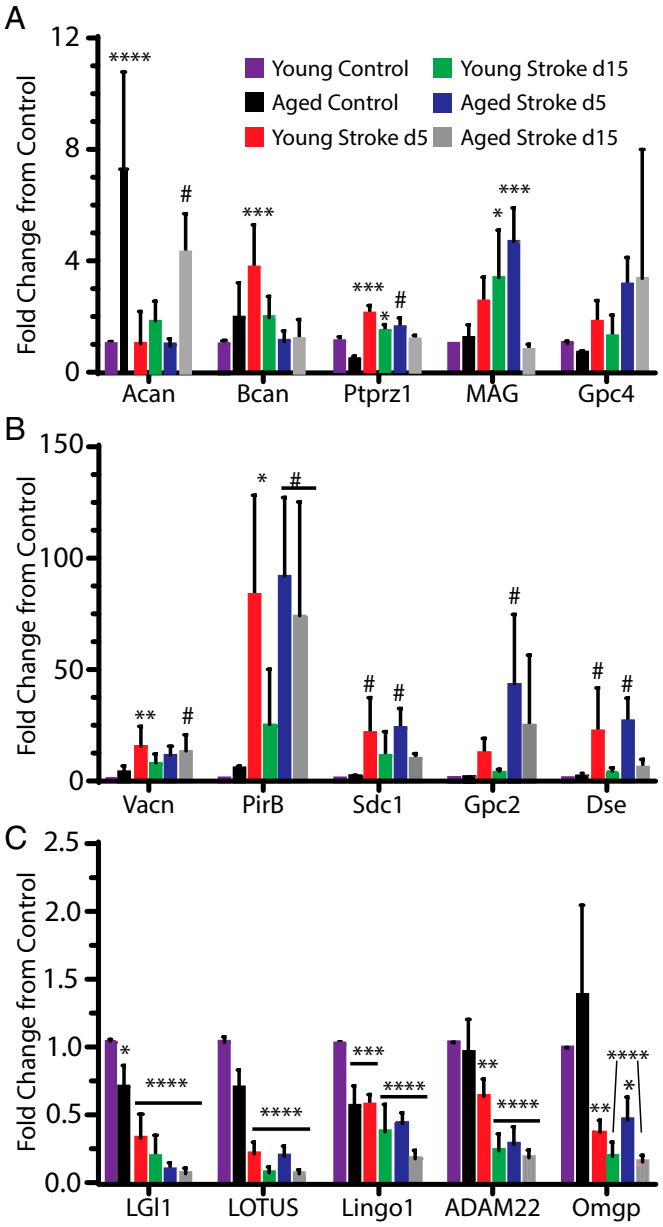

Fig. 6. Gene expression in myelin and ECM binding partners with NgR1. (*A–C*) qRT-PCR values from subcortical white matter from young adult and aged adult control samples (no stroke) and from day 5 and day 15 after stroke in young adult and aged adult white matter samples. Day 5 is the peak of OPC proliferation (Fig. 1*I*), and day 15 is the one significant time point of OPC differentiation block (Fig. 2 *G* and *H*). The *y* axis is fold change from the gene of interest in young adult control brain. $^{\#}P \leq 0.05$; $^{*}P \leq 0.01$; $^{**}P \leq 0.001$; $^{***}P \leq 0.0001$. See Table S1 for abbreviations.

promotes maturation of OPCs into OLs at the expense of their transformation into astrocytes.

White matter stroke is a disease of increasing age in humans, and aged mice exhibit a more severe motor deficit and poor recovery of function after white matter stroke (16). Because some of the changes in expression of NgR1 ligands and inhibitors were specific to the aged brains, we next determined whether a similar NgR1 ligand blockade in aged mice would translate into enhanced poststroke recovery. Aged mice received NgR(OMNI)-Fc that was either delivered directly into the stroke site as above, or in a more therapeutically relevant manner via continuous, 30-d systemic delivery after white matter stroke induction. NgR(OMNI)-Fc delivery resulted in a greater density of mature OL markers in white matter in the aged animals compared with Fc-treated controls (Fig. 7 *D–I*), which is in agreement with the enhanced OPC differentiation observed in the young adult OPC reporter NgR(OMNI)-Fc study. Blockade of NgR1 signaling can promote axonal sprouting after cortical or large artery stroke into or from areas of partial damage or axotomy (37–39). We labeled axonal connections that originate from the sensorimotor cortex that is just dorsal to the white matter stroke site or the homologous cortical area contralateral to the stroke using anterograde tracing with complimentary AAV injections (Fig. 8*A*). The virally labeled axons are clearly evident in the subcortical white matter both contralateral to the stroke and ipsilateral to the stroke site (Fig. 8*B*). There seemed to be more labeled axons in the stroke condition compared with either control brain or stroke+NgR(OMNI)-Fc (Fig. 8*B*). Quantification of cortical projections through the corpus callosum supports this appearance: There is a significant increase in cortical callosal projections after stroke, which is not seen with stroke+NgR(OMNI)-Fc (Fig. 8*C*). White matter stroke thus induces an axonal sprouting response that is blocked by NgR(OMNI)-Fc, possibly by this molecule's enhancement of oligodendrocyte differentiation.

In motor recovery tests, aged mice that received systemic delivery of NgR(OMNI)-Fc recovered motor control of the forelimb as measured with skilled reach and with gait, beginning at week 3 after stroke and were indistinguishable from nonstroke mice by week 5 after stroke (Fig. 8 *D* and *E*). Interestingly, a single direct injection of NgR(OMNI)-Fc into the infarct produced a transient recovery on weeks 2 and 3 after stroke that was then lost (Fig. 8*D*). To determine the effect of NgR1 ligand blockade on white matter structure during this period of behavioral recovery, myelination and axonal structure were determined with electron microscopy. The G ratio of myelin thickness to axonal diameter was diminished after stroke in young adult and aged white matter and partially (young adult) or fully restored to the control condition with NgR(OMNI)-Fc systemic treatment (Figs. 8 *F* and *G*). The relative percentage of unmyelinated axonal fibers was increased in subcortical white matter after white matter stroke in young adult (Fig. 8*G*), which increased to the total fiber density in white matter (Fig. S5). This increase in unmyelinated fibers was blocked by NgR(OMNI)-Fc (Fig. 8*G* and Fig. S5). This increase in unmyelinated fibers after stroke compared with control corresponds to the increase in virally traced cortical connections through the white matter (Fig. 8 *B* and *C*) and represents subcortical axonal sprouting, though there was no appearance of additional or ectopic axonal projections (Figs. 7 *F* and *K* and 8*B*) with features characteristic of axonal regeneration (40). Subcortical axonal sprouting was associated with decreased motor control of the affected forelimb in stroke (Fig. 8 *D* and *E*), and this process of axonal sprouting was prevented by NgR(OMNI)-Fc treatment, which improved functional recovery.

Thus, NgR1 ligand antagonism after white matter stroke induces white matter repair as defined by promoting a greater number of OLs, reduced OPC differentiation into astrocytes, increased myelination, reduced sprouting of unmyelinated cortical projections, and enhanced motor recovery. Prolonged treatment in the chronic stroke state improves recovery of motor control in aged animals at late time points after the stroke.

Discussion

Here, we show fundamental differences in white matter repair processes between white matter stroke and inflammatory and toxic white matter injuries. White matter stroke induces OPC proliferation and localization toward the lesion, but only a limited differentiation into OLs. These OPCs that react to the stroke are derived from local tissue progenitors rather than migration from the SVZ. A portion of the proliferating OPCs are shunted into astrocytes, particularly close to the stroke border. A similar differentiation potential is not seen in the noninjured white matter (Fig. 2*D* and also refs. 40 and 41), which indicates that specific

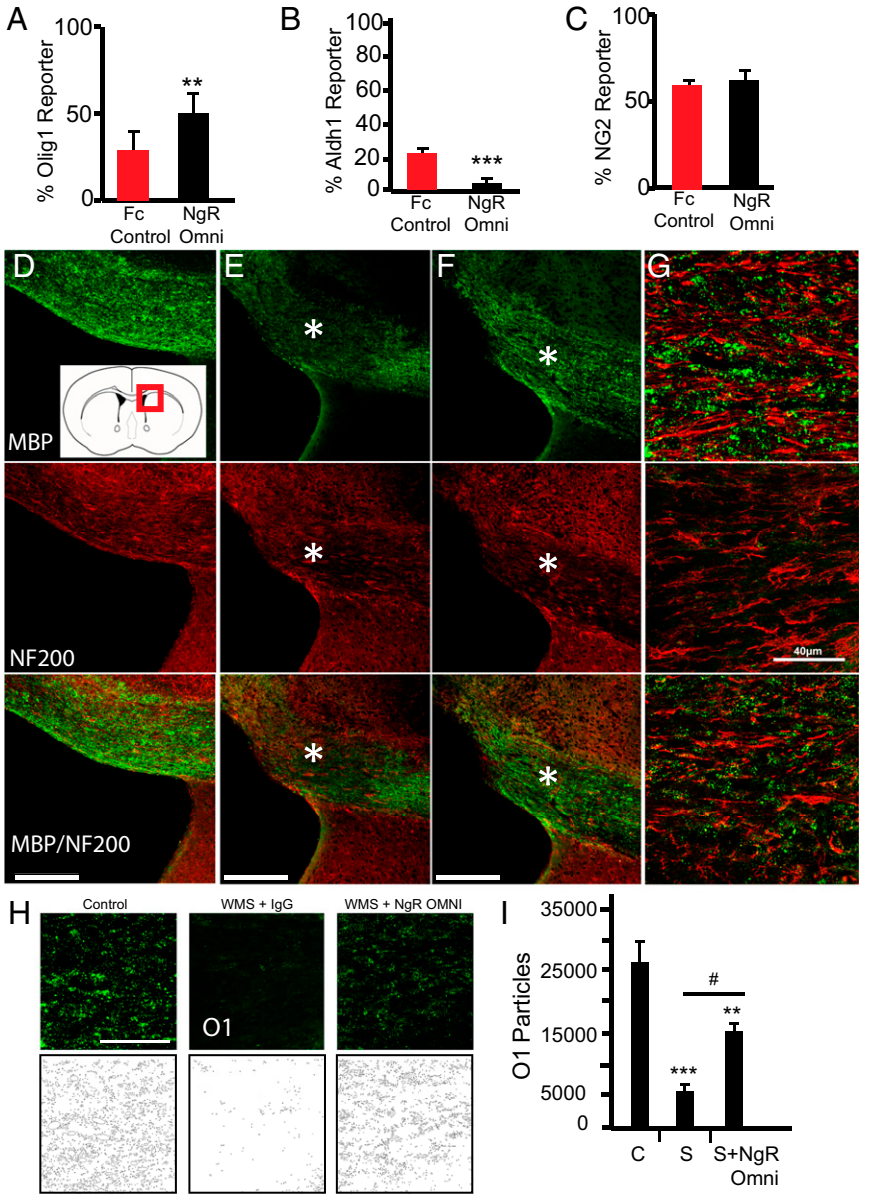

Fig. 7. NgR(OMNI)-Fc stimulates OPC differentiation. (*A–C*) Young adult WM stroke with NgR(OMNI)-Fc delivered into the stroke site 2 d after the stroke. (*A*) Percentage of differentiated reporters with Olig1 translocation. $^{**}P < 0.001$. (*B*) Percentage of cells expressing mature astrocyte marker Aldh1L1. $^{***}P < 0.0001$. (*C*) The percentage of immature $NG2^+$ reporter cells is not altered by NgR(OMNI)-Fc delivery. (*D–I*) Aged white matter stroke 9 wk after systemic infusion of NgR(OMNI)-Fc via minipump. Control, no stroke (*D*), stroke + Fc (*E*), and stroke+NgR(OMNI)-Fc (*F*) in aged mice 9 wk after stroke. (*D*, *Inset*) Location of micrographs. Asterisk indicates stroke. (Scale bars: *D–F*, 200 μm.) (*G*) Higher-magnification image of control white matter (*Top*), stroke + Fc (*Middle*), and stroke+NgR(OMNI)-Fc (*Bottom*). (Scale bar: 40 μm.) (*H*) Representative confocal images from subcortical white matter stained for O1 in control aged mice that were in the NgR(OMNI)-Fc long-term behavioral study. (*Top*) Images of O1 antibody staining. (*Bottom*) The corresponding images after highlighting all O1-positive particles. The count of O1-positive cellular elements was 38,595, 1,911, and 23,727, respectively, in these individual cases, which were used to produce the quantitative data in *I*. (Scale bar: 40 μm.) (*I*) Area of staining of $O1^+$ oligodendrocytes in aged subcortical white matter. C, control (no stroke) + Fc IgG; S, stroke + Fc IgG; S+NgROMNI, stroke + systemically delivered NgR(OMNI)-Fc.

molecular cues in the poststroke environment block OL regeneration and transform OPCs into astrocytes, contributing to the repair failure. Our data indicate that NgR1 ligands may block the production of mature OLs and that a related mechanism may play a role in the human disease, which is supported by two sets of findings: Select NgR1 ligands were induced after white matter stroke, particularly with aging, and sequestration of NgR1 ligands with NgR(OMNI)-Fc gave rise to OPC maturation and behavioral recovery in aged mice. In the present studies, systemic administration of NgR(OMNI)-Fc produced white matter repair and recovery in the peri-infarct zone and did so at chronic time points after the stroke, suggesting the possibility of a therapeutic delivery in this disease.

OPC Responses in White Matter Stroke vs. Other Lesions. There are striking contrasts of OPC regenerative responses between white matter stroke and other models of white matter injury. In MS patients, mouse models of MS, and rodent models of toxic demyelination, the process of OPC responsiveness to the injury can repair initial white matter lesions (8, 42). In human MS, about one-third of OPCs are in some transition toward mature OLs (42). We show that there is minimal progression of proliferating

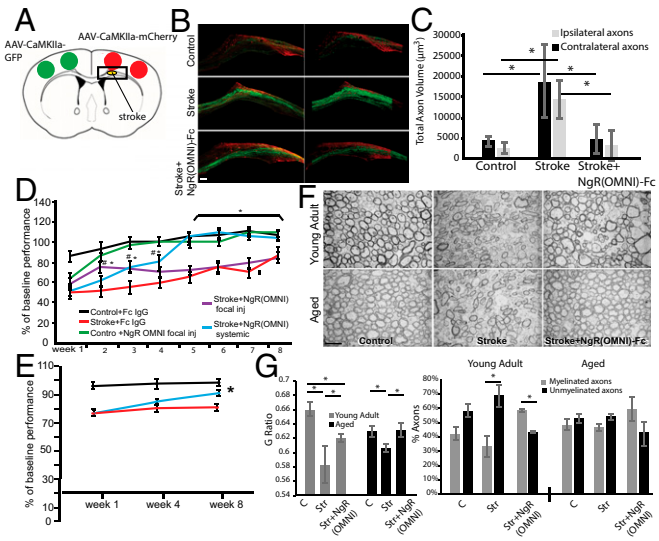

Fig. 8. Cortical connections and behavioral recovery after NgR1 blockade. (*A*) Schematic of AAV injection for anterograde tracing of callosal connections. The box shows location of images in *B*. (*B*) Images of corpus callosum in normal (control), stroke and stroke+NgR(OMNI)-Fc (delivered systemically) 4 wk after stroke. Virally labeled axons from the contralateral cortex are green; Virally labeled axons from the cortex dorsal to the stroke site (ipsilateral to stroke) are red. (*Left*) Confocal imaging of corpus callosum and (*Right*) segmentation of the axonal label for quantification shown in *C*. (Scale bar: 100 μm.) (*C*) Quantification of labeled axon fibers from contralateral and ipsilateral cortex to the stroke site. $*P < 0.05$ (two-way ANOVA, Tukey-Kramer post hoc). Data in *A*–*C* are from young adult mice. (*D*) Pasta skilled reaching task in aged mice. The *y* axis is the percent change from the testing session immediately prior to the stroke. $*P < 0.001$ compared with WMS-Fc and NGR-focal, $^{\#}P < 0.05$ NgR(OMNI)-Fc systemic compared with WMS-Fc. (*E*) Grid walking performance in aged mice. The *y* axis is percent change from the testing session immediately prior to the stroke. $*P = 0.018$ compared with WMS-Fc. (*F*) Electron microscopy of white matter in corpus callosum adjacent to the stroke site in age mice 8 wk after stroke. (Scale bar: 2 μm.) (*G*) Quantification of G ratio and percentages of myelinated and unmyelinated axons in white matter in corpus callosum adjacent to the stroke site 8 wk after stroke. $*P < 0.05$.

OPCs after white matter stroke into mature OLs, using both proliferation markers and genetic fate mapping. Interestingly, the initial OPC proliferation period is similar across toxic and stroked white matter lesions, with a maximum at day 5. However, in toxic white matter lesions, unlike white matter stroke, differentiation occurs early after the proliferative response because significant numbers of cells have markers of mature OLs at day 10 (27).

In toxic and inflammatory demyelinating lesions, an important source of the progenitor responses is the SVZ, with OPCs migrating out of the SVZ and into injured subcortical white matter (10, 27). Using viral vector labeling and proliferation markers that are timed for SVZ cell cycle kinetics (27), there was no migration of cells from the SVZ into white matter stroke, even though this stroke is near the SVZ and resembles in size the toxic demyelinating lesions that produce SVZ migration into white matter (10, 27). Thus, the equivalent location and size of stroke and primary demyelinating lesions did not produce equivalent SVZ migration, further indicating that the biologic response to focal white matter ischemia is different from toxic or inflammatory demyelination.

An Astrocytic Shunt and OPC Differentiation Block. Genetic fate mapping of OPCs after white matter stroke indicated that 4% to13% of these cells differentiate into astrocytes at any post-stroke time point examined. This finding is in agreement with published reports that demonstrate a bipotential nature of OPCs in vitro and in the presence of CNS injury (43, 44) although, in spinal cord injury, OPC differentiation into astrocytes is minimal (44). The astrocytic shunt of OPCs after white matter stroke may account for the very limited differentiation of OPCs into mature OLs, both directly via production of astrocytes instead of OLs and indirectly by producing a cell type that further inhibits OL production. Astrocytes inhibit OPC differentiation and promote astrocytic differentiation in vitro via BMP4 (45). However, BMP antagonists only partially prevent the ability of reactive astrocytes to block OPC differentiation. Other candidate factors implicated in astrocyte–OPC inhibitory interactions are hyaluronan (46) and Jagged-1 (47). The present data suggest another local inhibitory system for OPC differentiation in white matter stroke, in which NgR1 ligands inhibit OPC differentiation.

NgR1 Ligand Antagonism and White Matter Repair. Prominent extracellular factors that block OPC differentiation and white matter repair include myelin-associated inhibitory molecules, such as Nogo-A and MAG, as well as CSPGs (22, 45, 48). Myelin-associated molecules signal through NgR1 to -3 (49–51) and PirB (52). Expression of the interacting components in Nogo signaling is altered in many pathological conditions and in aging (33, 48, 53, 54). Nogo signaling has been studied for its role in axonal sprouting and recovery in cortical or large artery stroke, and its components have emerged as therapeutic targets in inflammatory demyelinating diseases (55). However, there are no previous studies of its action in white matter stroke or ischemic white matter repair. Expression analysis of NgR1-interacting molecules indicates that several NgR1 ligands (32) are induced after white matter stroke as a function of age, including aggrecan, versican, and the HSPG core proteins syndecan 1 and glypican 2. PirB, a receptor for myelin proteins that is active in many contexts with NgR1 (56), is remarkable in its 83× and 91× induction in the early stages of white matter stroke in young adult and aged brain, respectively. Endogenous inhibitors of NgR1 signaling, including LGl1, LOTUS, and ADAM22 (34, 35), are down-regulated after white matter stroke in the young adult and further down-regulated in the aged brain white matter after stroke. Many of these NgR1 ligands act through this receptor to decrease OPC differentiation, placing this signaling system as a candidate mediator for the differentiation block in OPC responses after white matter stroke.

To test the possibility that endogenous NgR1 ligands block axonal growth, OPC differentiation, and white matter repair after stroke, we delivered NgR(OMNI)-Fc (36) after both aged and young adult white matter stroke. NgR(OMNI)-Fc binds to NgR1 ligands and perturbs their binding to NgR1, NgR2, NgR3, PirB, and possibly several other receptors. Antagonism of NgR1 ligands promotes OPC differentiation into cells positive for markers of mature OLs in both young adult and aged brains and promotes functional recovery of motor control after white matter stroke in aged animals. Importantly, this effect on behavioral recovery was produced at chronic time points after the stroke, and via systemic delivery of NgR(OMNI)-Fc. The systemic delivery of a large protein such as NgR(OMNI)-Fc is likely effective in the CNS because similar-sized mouse serum IgG also penetrated into the brain around the stroke site (Fig. 1*B*). As such, NgR1 ligands may influence OPC differentiation in several ways. NgR(OMNI)-Fc may perturb Lingo-1 signaling (53), interfere directly with Nogo-A function (31), or complex with and neutralize currently unknown inhibitors of OPC differentiation.

Antibody blockade of Lingo-1 promotes OPC differentiation into mature oligodendrocytes (51) and has entered into clinical trials for recovery in MS (55). Nogo signaling also blocks axonal sprouting after CNS lesions. In stroke, several antagonists to NgR1 signaling promote axonal sprouting and functional recovery (37–39). These past studies of NgR1 signaling differ substantially with the present findings. The previous studies examined neuronal sprouting in large artery or cortical stroke models whereas the present study was focused on OPC responses and repair of white

matter stroke damage involving remyelination of surviving axons in peri-infarct white matter. Detailed analysis of regions of partial axonal damage after white matter stroke after NgR(OMNI)-Fc administration does not show enhanced axonal growth. However, in many cases, axonal sprouting can occur within existing neuronal networks and requires detailed mapping studies (38, 57, 58). Future studies will need to systematically map the cortical connections of brain regions that might project through the ischemic white matter to determine whether distant axonal sprouting occurs in these types of stroke in the presence of NgR(OMNI)-Fc.

In summary, the present findings show that white matter stroke results in a unique white matter environment compared with other mechanisms of white matter injury. This environment alters the differentiation potential and fate of OPCs. Stroke-specific inhibition of repair is at least in part mediated by NgR1 ligands, some of which show a dramatic increase in aged brains. The negative effects of NgR1 ligands can be reversed in a clinically relevant manner via systemic delivery of NgR(OMNI)-Fc in chronic stroke to promote functional recovery, even in aged brains.

Materials and Methods

Mice. All experiments were approved by the University of California, Los Angeles Chancellor's Animal Research Committee. Heterozygous Ng2::CreERT2 (gift from Akiko Nishiyama, University of Connecticut, Storrs, CT) were crossed with R26R-eYFP reporter mice (The Jackson Laboratory) to obtain the OPC reporter mouse line NG2::CreERT2/R26R-eYFP animals. Mice older than 2.5 mo received i.p. injections of the tamoxifen derivative 4OHT (10 mg; dissolved at 10 mg/mL in a 1:9 ethanol/corn oil mixture; Sigma) twice for 5 d. Mice were subjected to white matter stroke or sham procedure 10 d after the last dose of 4OHT. Brains were collected at 4, 7, 10, and 14 d after stroke or sham for cell fate-mapping experiments (n = 5 to 6 per cohort). In NgR(OMNI)-Fc/Human IgG Fc studies, the OPC reporter mice were treated with 4OHT in the same manner, and brains were isolated 14 d after stroke or sham for fate mapping (n = 5 per cohort). Paraformaldehyde/lysine/periodate (PLP)-GFP reporter and YFP-H transgenic mice were used to assess the loss of mature oligodendrocytes and axons, respectively (The Jackson Laboratory). Aged mice (24 mo) were obtained from the National Institute on Aging. For OPC proliferation experiments, EdU (Life Technologies) was administered [0.3 mg/10 g of mouse weight (1 mg/mL), i.p.] twice 24 h before euthanasia time points of 4, 7, 10, and 14 d after stroke or sham (n = 5 per cohort). All experiments were performed in accordance with National Institutes of Health animal protection guidelines and were approved by the University of California, Los Angeles Animal Research Committee.

White Matter Stroke. White matter stroke was produced as described (15, 16). Briefly, N5-(1-Iminoethyl)-L-ornithine (L-NIO; 27 mg/mL in sterile physiological saline; EMD/Millipore) was injected via micropipette through the cortex at an angle of 36° with a dorso-medial to ventro-lateral injection path, into the white matter underlying the forelimb motor cortex. Three stereotaxic injections (each of 200 nL of L-NIO solution) were made in the following coordinates: anteroposterior (A/P), +0.22, +0.74, +1.24; mediolateral (M/L), +0.20, +0.17, +0.15; dorsoventral (D/V), −2.20, −2.25, −2.30. Control animals underwent craniotomy alone. Aged mice received three injections of L-NIO at A/P, +0.5, 0, −0.5; M/L, −0.96 (for all three injections); D/V, −1.2, −1.15, −1.1; at an angle of 45° with a dorso-posterior to ventro-anterior injection path.

Immunohistochemistry. Immunohistochemistry was performed as described (13, 16). For immunohistochemical studies using NG2 staining, animals were perfused transcardially with 0.1 M PBS followed by PLP fixative containing 2% (wt/vol) paraformaldehyde. For studies not involving NG2 staining, standard 4% paraformaldehyde perfusions were used. Brains were cryoprotected in 30% (wt/vol) sucrose brains, frozen, and sectioned into four series of 40-μm sections. Sections were blocked in 5% (vol/vol) donkey serum, incubated with a primary antibody overnight at 4 °C, incubated with a secondary antibody for 1 h at room temperature, and coverslipped. For immunostaining with antibodies raised in the mouse, a Mouse on Mouse kit was used to eliminate nonspecific binding (Vector). Primary antibodies were as follows: goat anti GFP (1:5,000; gift from Nathaniel Heintz, The Rockefeller University, New York), rabbit anti–Iba-1 (1:1,000; Wako Chemicals), rabbit NG2 (1:200; Millipore), rat anti-myelin basic protein (MBP) (1:1,000, EMD Millipore), rabbit anti-Olig2 (1:500; EMD Millipore), rat anti-Olig1 (gift from Bennett Novitch, University of California, Los Angeles), mouse anti-O1 (EMD Millipore), rabbit anti–GST-π (1:500; Abcam), rabbit anti-CC1 (1:100; EMD Millipore). rabbit anti-Aldh1 (1:1,000; Abcam), rabbit anti-Caspr (1:500; Abcam), mouse anti–βIV-spectrin (1:200; Neuromab), goat anti–PDGF-Rβ (1:100; R&D Systems), Dcx, (1:400, C18; Santa Cruz), and NF200 (1;500, N4142; Sigma). All secondary antibodies were donkey F(ab)2 fragments conjugated to cy2, cy3, or cy5 (Jackson Immunoresearch) and were used at a dilution of 1:500. EdU incorporation was detected by the Click-iT EdU cell proliferation assay following the kit protocol (Life Technologies). To determine the initial degrees of BBB disruption in this model, brain sections 7 d after the stroke were stained for mouse IgG, normally not present via immunohistochemical staining in mouse brain.

Viral Tracing Studies. Changes in axonal density after stroke were assessed using four intracortical injections of two different adeno-associated virus. Three cohorts of six mice [control, stroke, and stroke+NgR(OMNI)-Fc] received two 1-μL injections of AAV-CaMKIIa-mCherry (University of North Carolina Vector Core) into the ipsilateral sensorimotor cortex and two 1-μL injections AAV-CaMKIIa-GFP (University of North Carolina Vector Core) into the contralateral sensorimotor cortex (both done at the time of the stroke) at an angle of 10°, using the following coordinates: ML, +1.5; DV, −0.74; and ML, +3, DV, −0.74. Mice were killed 4 wk after stroke. All brains were fixed, frozen, and coronally sectioned 40 μm apart (CM0530; Leica Biosystems). A series of six sections spaced 200 μm apart were mounted and coverslipped with DPX mounting medium (EMS). A large-scale image of the entire white matter was acquired using a 20× objective with confocal microscopy (Nikon C2). The parameters for scanning were kept constant across treatment conditions. A 3D analysis on Imaris Imaging software (Version 8.1.1; Bitplane) was performed by creating two different surfaces: (*i*) for AAV-CaMKIIa-mCherry–positive axons and (*ii*) for AAV-CaMKIIa-GFP–positive axons.

EM Studies. Two different cohorts of 12 mice [young mice (3 mo old) and aged mice (24 mo old)] were divided into three different groups each: Control, stroke, and stroke+NgR(OMNI)-Fc. All mice underwent intravascular perfusion with a fixative solution containing 2% paraformaldehyde and 2% glutaraldehyde. The brain was removed and postfixed overnight in the fixative solution at 4 °C. Brains were sectioned in the parasagittal plane, and the peri-infarct white matter was identified and blocked. The tissue blocks were rinsed in phosphate-buffered saline (PBS), osmicated, dehydrated in ethanol, and embedded in Epon (Electron Microscope Sciences).

Semithin sections (0.5- to 1.0-μm thickness) were cut using an RMC Products PowerTome ultramicrotome (Boeckeler Instruments) and stained with toluidine blue for light microscopic identification of the peri-infarct white matter. A Nikon E600 light microscope equipped with a camera lucida reconstruction tube was used to create trimming maps and select the region of interest. Ultrathin sections (60- to 90-nm thickness) of the peri-infarct white matter were cut using an RMC Products PowerTome ultramicrotome, and the sections were collected on formvar-coated one-hole copper grids. The sections were next contrasted using uranyl acetate and lead citrate solutions.

Ultrathin sections were examined in a JEOL 100CX transmission electron microscope. Electron micrographs were taken at a 7,200× magnification. Images were scanned, and representative regions of interest, corresponding to approximate white matter areas of 130 μm^2, were analyzed quantitatively. All myelinated axons within the region of interest were included in the studies for each animal. A computer equipped with ImageJ (https://imagej.nih.gov/ij/) was used to measure the cross-sectional area for each myelinated fiber and the corresponding area for its axon proper. The formula for a circle was used to calculate the diameter for each measured area. The G-ratio was determined by dividing the axon diameter with the fiber diameter for each myelinated fiber.

In both AAV tracing studies and in EM analysis, data were tested with one-way analysis of variance (ANOVA) with level of significance set at $P < 0.05$ with Tukey's honest significant difference (HSD) test.

qRT-PCR Analysis of NgR1-Associated Molecules. qPCR was performed on fresh tissue samples. Brains were immersed in cold PBS for 5 min, and an ∼1-mm^3 segment of white matter containing the stroke, or the equivalent area in control animals, was manually dissected out. Total RNA was isolated using the Qiagen RNeasy Micro Kit according to the manufacturer's instructions. Then, 500 ng of RNA from each sample were subjected to reverse transcriptase reaction with SuperScript III Reverse Transcriptase from Life Technologies. For Fluidigm Real-Time PCR, 1 μL of each cDNA solution was used to generate a preamp mix with TaqMan Pre-Amp Master Mix (Life Technologies). Preamp mixes were prepared and run for 15 cycles and cleaned up with ExoSnap (SelectScience). Preamp reaction mixes were diluted 15× in DNA Suspension Buffer (Teknova) and run on a Fluidigm Real-Time system. NgR1 expression was detected using a Roche LightCycler 480 SYBR Green I

Master kit and Roche LightCycler 480 Real-Time PCR System. Preamp samples were prepared as for Fluidigm Real-Time PCR analysis. For NgR1 expression analysis, PCR was run with 1 μL of undiluted preamp whereas preamp samples for the detection of housekeeping gene G3PDH were diluted 30×.

NgR(OMNI)-Fc Delivery. The production and characterization of NgR(OMNI)-Fc has been described elsewhere (36). A soluble form of NgR(OMNI)-Fc that lacks the proteoglycan binding motif m2 (32, 36) was transiently expressed in HEK293 cells and affinity purified using protein A/G beads. Proper folding of purified NgR(OMNI)-Fc was confirmed by binding to myelin inhibitors as described (36). For in vivo studies, 1.05 μg of NgR(OMNI)-Fc or human IgG Fc (Jackson Immunoresearch) were delivered into white matter stroke lesions 2 d after stroke induction at the following coordinates in millimeters: A/P, +0.50, +1.05; M/L, +1.95, +1.75; D/V, −1.30, −1.35. In the reporter mice, tissue was analyzed 14 d after stroke. For behavioral studies in adult and aged animals, NgR(OMNI)-Fc was directly injected into the stroke site as in the OPC reporter mice or given systemically: NgR(OMNI)-Fc was delivered in a month-long infusion via two minipumps (1002; Alzet) placed in the subdermal space between the scapulae. Each pump delivered 6 μL/d × 14 d × 4.6 mg/mL NgR (OMNI)-Fc × two pumps per mouse (the second pump replaced the first on day 14), which equaled 0.77 mg of total dose per mouse over 28 d.

Microscopy and Stereology. Stereology (Stereoinvestigator; MBF Bioscience) was carried out on Z stack confocal images (Nikon C2 confocal), exported for offline analysis. Cells of interest were stereologically quantified using the optical fractionator probe and neuroanatomical quantification. Briefly, a counting area was drawn to include the lesion with adjacent peri-infarct white matter of each section analyzed. Four serial sections spaced 240 μm apart were used to estimate the total number of cells of interest in each brain. For tissue analysis in aged mice after behavioral studies, subcortical white matter medial to the stroke site was stained for O1 and NF200 (above), and then a region of interest was scanned (20×, Nikon C2 confocal) and analyzed for total O1 staining with particle analysis (ImageJ). Axon number was quantified using a line scan orthogonally in confocal image stacks through the subcortical white matter at varying distances from the infarct.

Behavior. The pasta matrix task was performed as described previously (16). Mice were trained daily before stroke to reach and retrieve small pieces of vertically oriented capellini pasta from a grid arrangement. Only mice that consistently retrieved more than six pieces per 10-min session were used in the study. After stroke, the mice were tested weekly, and performance (i.e., number of pasta pieces retrieved) was compared with the prestroke performance. The grid-walking task was performed as previously described (57–59) on a separate cohort of control, stroke, and stroke+NgR(OMNI)-Fc mice. The total number of foot faults as well as the total number of correct, nonfootfault steps were counted, and a correct step percentage was calculated. Mice were tested in the grid-walking task once before the stroke to establish baseline performance levels, and then retested 1 wk, 1 mo, and 2 mo after stroke induction.

Human Studies. Human studies were conducted on autopsy material, which does not require institutional review board approval, as published in Hinman et al. (60). The cases selected for examination in this study are autopsy cases from a clinicopathologic study of cognitively normal subjects, those with subcortical ischemic vascular dementia (SIVD), or Alzheimer's disease (AD) participants. Written informed consent for autopsy was obtained from all subjects or legal next-of-kin. From this larger database, cases selected for detailed microscopy included those with definable small vessel infarcts determined by expert neuropathologic assessment of H&E-stained sections. Demographic information and anatomic location of infarcts for each case are detailed in Hinman et al. (15). In addition, postmortem tissue examination of two subjects with a genetically confirmed diagnosis of autosomal dominant retinal vasculopathy with cerebral leukodystrophy (RVCL) [formerly hereditary endotheliopathy with retinopathy, nephropathy, and stroke (HERNS)] syndrome were also included in the study by Jen et al. (61).

Autopsy and brain extractions were performed according to standard procedures. Extracted brains were immediately fixed in 10% formalin for 2 wk. Fixed specimens were then blocked for regions of interest, processed, and embedded in paraffin. Six-micrometer-thick tissue sections were generated from the paraffin-embedded blocks for histologic analysis using immunofluorescent labeling as follows. Sections were first baked at 60 °C to melt the paraffin wax and subsequently washed in xylenes to dissolve residual paraffin, followed by graded ethanol baths (100% to 70%) and ddH_2O to rehydrate the tissue. For histologic staining, sections were then immersed in Harris Hematoxylin (Fisher) for 1 min and slightly destained in 1% HCl in 80% ethanol. Hematoxylin-stained slides were further developed with 0.2% ammonia water and then immersed in eosin-Y (Fisher) for 3 min. After eosin immersion, sections were dehydrated in graded ethanol baths (70% to 100%), cleared in xylenes, and coverslipped for visualization via light microscopy.

For immunohistochemical labeling, tissue epitopes were exposed with heat-induced antigen retrieval using a pressurized antigen-decloaking chamber at 120 °C for 5 min in 10 mmol citrate, pH 6.0, and allowed to cool to room temperature. After antigen retrieval, tissue sections were permeabilized with 0.3% Triton X-100 in PBS followed by 5% acetic acid in 95% ethanol. After permeabilization, sections were blocked with 5% normal donkey serum, 0.3% Triton X-100 in PBS (NDSX) for 1 h. Finally, sections were incubated overnight sequentially with the following primary antibodies: rabbit anti-versican (AB177480, 1:50; Abcam), rabbit anti-DSE (10452-1-AP, 1:50; Protein Techm), PirB (AB2269, 1:60; Millipore). Antibody staining was visualized with diamino benzidine (DAB).

Statistical Analysis. All studies were analyzed with investigators blinded to treatment condition. Tissue outcome and behavioral studies were powered based on means and SDs in related work (13, 15, 16) predicted to be sufficient to detect a statistically significant result in ANOVA with $\alpha = 0.05$ and power > 0.8. Data were tested with multiple comparisons ANOVA and Bonferroni or Tukey–Kramer post hoc testing (Graphpad Prism).

ACKNOWLEDGMENTS. We thank Michael Reitman, Bradley Hagan, and Spencer Tung for technical assistance. Research was funded by National Institute of Neurological Disorders and Stroke Grants F31NS076025 and NS07752, the Dr. Miriam and Sheldon G. Adelson Medical Research Foundation, and the American Stroke Association–Bugher Foundation.

1. de Leeuw FE, et al. (2001) Prevalence of cerebral white matter lesions in elderly people: A population based magnetic resonance imaging study. The Rotterdam Scan Study. *J Neurol Neurosurg Psychiatry* 70(1):9–14.
2. Schneider AT, et al. (2004) Ischemic stroke subtypes: A population-based study of incidence rates among blacks and whites. *Stroke* 35(7):1552–1556.
3. Iadecola C (2013) The pathobiology of vascular dementia. *Neuron* 80(4):844–866.
4. DeCarli C, Fletcher E, Ramey V, Harvey D, Jagust WJ (2005) Anatomical mapping of white matter hyperintensities (WMH): Exploring the relationships between periventricular WMH, deep WMH, and total WMH burden. *Stroke* 36(1):50–55.
5. Schmidt R, et al. (2004) White matter lesion progression: A surrogate endpoint for trials in cerebral small-vessel disease. *Neurology* 63(1):139–144.
6. Zheng JJ, Delbaere K, Close JC, Sachdev PS, Lord SR (2011) Impact of white matter lesions on physical functioning and fall risk in older people: A systematic review. *Stroke* 42(7):2086–2090.
7. Debette S, Markus HS (2010) The clinical importance of white matter hyperintensities on brain magnetic resonance imaging: Systematic review and meta-analysis. *BMJ* 341:c3666.
8. Gallo V, Armstrong RC (2008) Myelin repair strategies: A cellular view. *Curr Opin Neurol* 21(3):278–283.
9. Huang JK, Franklin RJ (2012) Current status of myelin replacement therapies in multiple sclerosis. *Prog Brain Res* 201(2):219–231.
10. Menn B, et al. (2006) Origin of oligodendrocytes in the subventricular zone of the adult brain. *J Neurosci* 26(30):7907–7918.
11. Etxeberria A, Mangin JM, Aguirre A, Gallo V (2010) Adult-born SVZ progenitors receive transient synapses during remyelination in corpus callosum. *Nat Neurosci* 13(3):287–289.
12. McIver SR, et al. (2010) Oligodendrocyte degeneration and recovery after focal cerebral ischemia. *Neuroscience* 169(3):1364–1375.
13. Sozmen EG, Kolekar A, Havton LA, Carmichael ST (2009) A white matter stroke model in the mouse: Axonal damage, progenitor responses and MRI correlates. *J Neurosci Methods* 180(2):261–272.
14. Sozmen EG, Hinman JD, Carmichael ST (2012) Models that matter: White matter stroke models. *Neurotherapeutics* 9(2):349–358.
15. Hinman JD, Rasband MN, Carmichael ST (2013) Remodeling of the axon initial segment after focal cortical and white matter stroke. *Stroke* 44(1):182–189.
16. Rosenzweig S, Carmichael ST (2013) Age-dependent exacerbation of white matter stroke outcomes: A role for oxidative damage and inflammatory mediators. *Stroke* 44(9):2579–2586.
17. Wardlaw JM, et al. (2013) Blood-brain barrier permeability and long-term clinical and imaging outcomes in cerebral small vessel disease. *Stroke* 44(2):525–527.
18. Arnett HA, et al. (2004) bHLH transcription factor Olig1 is required to repair demyelinated lesions in the CNS. *Science* 306(5704):2111–2115.
19. Göritz C, et al. (2011) A pericyte origin of spinal cord scar tissue. *Science* 333(6039):238–242.
20. Aguirre A, Gallo V (2004) Postnatal neurogenesis and gliogenesis in the olfactory bulb from NG2-expressing progenitors of the subventricular zone. *J Neurosci* 24(46):10530–10541.
21. Monteiro de Castro G, Deja NA, Ma D, Zhao C, Franklin RJ (2015) Astrocyte activation via Stat3 signaling determines the balance of oligodendrocyte versus Schwann cell remyelination. *Am J Pathol* 185(9):2431–2440.
22. Zawadzka M, et al. (2010) CNS-resident glial progenitor/stem cells produce Schwann cells as well as oligodendrocytes during repair of CNS demyelination. *Cell Stem Cell* 6(6):578–590.

23. Wrabetz L, Feltri ML (2001) Do Schwann cells stop, DR(o)P2, and roll? *Neuron* 30(3): 642–644.
24. Gensert JM, Goldman JE (1997) Endogenous progenitors remyelinate demyelinated axons in the adult CNS. *Neuron* 19(1):197–203.
25. Ohab JJ, Fleming S, Blesch A, Carmichael ST (2006) A neurovascular niche for neurogenesis after stroke. *J Neurosci* 26(50):13007–13016.
26. Psachoulia K, Jamen F, Young KM, Richardson WD (2009) Cell cycle dynamics of NG2 cells in the postnatal and ageing brain. *Neuron Glia Biol* 5(3-4):57–67.
27. Jablonska B, et al. (2010) Chordin-induced lineage plasticity of adult SVZ neuroblasts after demyelination. *Nat Neurosci* 13(5):541–550.
28. Kotter MR, Stadelmann C, Hartung HP (2011) Enhancing remyelination in disease: Can we wrap it up? *Brain* 134(Pt 7):1882–1900.
29. Harlow DE, Macklin WB (2014) Inhibitors of myelination: ECM changes, CSPGs and PTPs. *Exp Neurol* 251(1):39–46.
30. Yuen TJ, et al. (2014) Oligodendrocyte-encoded HIF function couples postnatal myelination and white matter angiogenesis. *Cell* 158(2):383–396.
31. Chong SY, et al. (2012) Neurite outgrowth inhibitor Nogo-A establishes spatial segregation and extent of oligodendrocyte myelination. *Proc Natl Acad Sci USA* 109(4):1299–1304.
32. Dickendesher TL, et al. (2012) NgR1 and NgR3 are receptors for chondroitin sulfate proteoglycans. *Nat Neurosci* 15(5):703–712.
33. VanGuilder Starkey HD, Bixler GV, Sonntag WE, Freeman WM (2013) Expression of NgR1-antagonizing proteins decreases with aging and cognitive decline in rat hippocampus. *Cell Mol Neurobiol* 33(4):483–488.
34. Thomas R, et al. (2010) LGI1 is a Nogo receptor 1 ligand that antagonizes myelin-based growth inhibition. *J Neurosci* 30(19):6607–6612.
35. Sato Y, et al. (2011) Cartilage acidic protein-1B (LOTUS), an endogenous Nogo receptor antagonist for axon tract formation. *Science* 333(6043):769–773.
36. Robak LA, et al. (2009) Molecular basis of the interactions of the Nogo-66 receptor and its homolog NgR2 with myelin-associated glycoprotein: Development of NgROMNI-Fc, a novel antagonist of CNS myelin inhibition. *J Neurosci* 29(18):5768–5783.
37. Lee JK, Kim JE, Sivula M, Strittmatter SM (2004) Nogo receptor antagonism promotes stroke recovery by enhancing axonal plasticity. *J Neurosci* 24(27):6209–6217.
38. Li S, et al. (2010) An age-related sprouting transcriptome provides molecular control of axonal sprouting after stroke. *Nat Neurosci* 13(12):1496–1504.
39. Lindau NT, et al. (2014) Rewiring of the corticospinal tract in the adult rat after unilateral stroke and anti-Nogo-A therapy. *Brain* 137(Pt 3):739–756.
40. Steward O, Zheng B, Tessier-Lavigne M (2003) False resurrections: Distinguishing regenerated from spared axons in the injured central nervous system. *J Comp Neurol* 459(1):1–8.
41. Dimou L, Simon C, Kirchhoff F, Takebayashi H, Götz M (2008) Progeny of Olig2-expressing progenitors in the gray and white matter of the adult mouse cerebral cortex. *J Neurosci* 28(41):10434–10442.
42. Kuhlmann T, et al. (2008) Differentiation block of oligodendroglial progenitor cells as a cause for remyelination failure in chronic multiple sclerosis. *Brain* 131(Pt 7):1749–1758.
43. Zhu X, Bergles DE, Nishiyama A (2008) NG2 cells generate both oligodendrocytes and gray matter astrocytes. *Development* 135(1):145–157.
44. Kondo T, Raff M (2000) Oligodendrocyte precursor cells reprogrammed to become multipotential CNS stem cells. *Science* 289(5485):1754–1757.
45. Hampton DW, et al. (2007) A potential role for bone morphogenetic protein signalling in glial cell fate determination following adult central nervous system injury in vivo. *Eur J Neurosci* 26(11):3024–3035.
46. Back SA, et al. (2005) Hyaluronan accumulates in demyelinated lesions and inhibits oligodendrocyte progenitor maturation. *Nat Med* 11(9):966–972.
47. Zhang Y, et al. (2009) Notch1 signaling plays a role in regulating precursor differentiation during CNS remyelination. *Proc Natl Acad Sci USA* 106(45):19162–19167.
48. Galtrey CM, Fawcett JW (2007) The role of chondroitin sulfate proteoglycans in regeneration and plasticity in the central nervous system. *Brain Res Brain Res Rev* 54(1): 1–18.
49. Mi S, et al. (2005) LINGO-1 negatively regulates myelination by oligodendrocytes. *Nat Neurosci* 8(6):745–751.
50. Huang JY, et al. (2012) Expression and function of myelin-associated proteins and their common receptor NgR on oligodendrocyte progenitor cells. *Brain Res* 1437(1): 1–15.
51. Mi S, et al. (2007) LINGO-1 antagonist promotes spinal cord remyelination and axonal integrity in MOG-induced experimental autoimmune encephalomyelitis. *Nat Med* 13(10):1228–1233.
52. Atwal JK, et al. (2008) PirB is a functional receptor for myelin inhibitors of axonal regeneration. *Science* 322(5903):967–970.
53. Buser JR, et al. (2012) Arrested preoligodendrocyte maturation contributes to myelination failure in premature infants. *Ann Neurol* 71(1):93–109.
54. Sobel RA, Ahmed AS (2001) White matter extracellular matrix chondroitin sulfate/dermatan sulfate proteoglycans in multiple sclerosis. *J Neuropathol Exp Neurol* 60(12):1198–1207.
55. Mi S, Pepinsky RB, Cadavid D (2013) Blocking LINGO-1 as a therapy to promote CNS repair: From concept to the clinic. *CNS Drugs* 27(7):493–503.
56. Akbik F, Cafferty WB, Strittmatter SM (2012) Myelin associated inhibitors: A link between injury-induced and experience-dependent plasticity. *Exp Neurol* 235(1):43–52.
57. Clarkson AN, et al. (2011) AMPA receptor-induced local brain-derived neurotrophic factor signaling mediates motor recovery after stroke. *J Neurosci* 31(10):3766–3775.
58. Overman JJ, et al. (2012) A role for ephrin-A5 in axonal sprouting, recovery, and activity-dependent plasticity after stroke. *Proc Natl Acad Sci USA* 109(33):E2230–E2239.
59. Clarkson AN, Huang BS, Macisaac SE, Mody I, Carmichael ST (2010) Reducing excessive GABA-mediated tonic inhibition promotes functional recovery after stroke. *Nature* 468(7321):305–309.
60. Hinman JD, Lee MD, Tung S, Vinters HV, Carmichael ST (2015) Molecular disorganization of axons adjacent to human lacunar infarcts. *Brain* 138(3):736–745.
61. Jen J, et al. (1997) Hereditary endotheliopathy with retinopathy, nephropathy, and stroke (HERNS). *Neurology* 49(5):1322–1330.